CrossMark

Numerical reconstruction of trajectory of small-size surface drifter in the Mediterranean sea

Reconstruction of surface drift in the Mediterranean sea

Elena Y. Shchekinova[1,2] · Yogesh Kumkar[1] · Giovanni Coppini[1]

Abstract In this study, we addressed the effects of wind-induced drift on Lagrangian trajectories of surface sea objects using high-resolution ocean forecast and atmospheric data. Application of stochastic Leeway model for prediction of trajectories drift was considered for the numerical reconstruction of the Elba accident that occurred during the period 21.06.2009–22.06.2009: a person on an inflatable raft was lost in the vicinity of the Elba Island coast; from the initial position, the person on a raft drifted southwards in the open sea and later he was found on a partially deflated raft during rescue operation. For geophysical forcing, we used high-resolution currents from the Mediterranean Forecasting System and atmospheric wind from the European Centre for Medium-Range Weather Forecasts. To investigate the effect of wind on trajectory behavior, numerical simulations were performed using different categories of drifter-like particles similar to a person on an inflatable raft. An algorithm of spatial clustering was used to differentiate the most probable search areas with a high density of particles. Our results showed that the simulation scenarios using particles with characteristics of draft-limited sea drifters provided better prediction of an observed trajectory in terms of the probability density of particles.

Responsible Editor: Richard Signell

✉ Elena Y. Shchekinova
shchekinova.elena@gmail.com

[1] Euro–Mediterranean Center for Climate Change, via Augusto Imperatore 16, 73100 Lecce, Italy

[2] Institute of Physics, Southern Federal University, Stachki, 194, 344110, Rostov on Don, Russia

1 Introduction

Numerical approaches for the forecast of sea drifters frequently deal with uncertainties of the sea object parameterization due to changing atmospheric surface wind (Kirwan et al. 1975; Allen and Plourde 1999). In addition, the lack of high-resolution ocean and atmospheric data (OD́onnell et al. 2005; Davidson et al. 2009) often leads to low-quality prediction. Advances in high-resolution operational forecast (Pinardi et al. 2003; Oddo et al. 2006; Tonani et al. 2008) for the Mediterranean Sea provided a framework for a more accurate prediction of drifters forecast in this area. Also, the inclusion of assimilation data schemes (Dobricic et al. 2004; Dobricic and Pinardi 2008) improved the prediction of time-dependent currents and wind in comparison to earlier models.

A large databank of windage characteristics of sea objects was collected over the years (Allen 2005; Allen et al. 2010) that uncovered a linear relationship between drift velocity and applied surface wind for different categories of sea drifters. These field observations were used for the trajectory prediction in the stochastic approach (Hackett et al. 2006; Breivik and Allen 2008; Breivik et al. 2012). The stochastic Leeway model (Breivik and Allen 2008) produced final positions of sea objects based on their windage characteristics (Allen and Plourde 1999) and predicted search areas in terms of probability densities. However, the model was not capable to classify the sea floaters according to their temporal and spatial behavior. While backtracking procedure could provide such classification, it
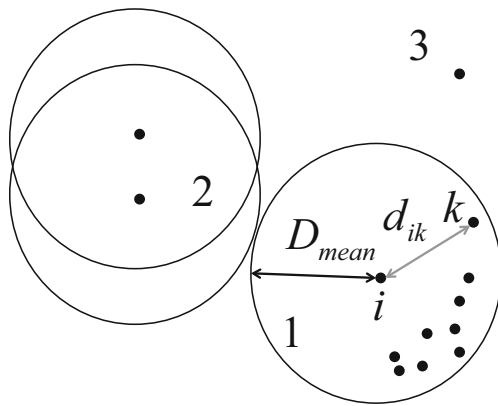
Fig. 1 Schematic representation of clustering algorithm. Three groups of particles are shown: (1) the ith and kth particles with separation distance $d_{ik} < D_{mean}$ and their neighbors form one cluster, (2) no cluster is formed, (3) isolated particle. The minimum number of particles per cluster $N_{min} = 10$

is computationally expensive and could not be used in real applications.

As an alternative to the above methods, here we used a faster computational approach for characterization of drifters in a large ensemble. It is based on a density clustering algorithm (Ester et al. 1996). It was designed to improve qualitative information about the stochastic outcome of the Leeway simulations (Breivik and Allen 2008; Breivik et al. 2012) and to increase the quality of prediction. The method of spatial clustering provides better localization of the areas of higher probability density and finds possible particles–outliers. Also, the procedure allows sorting out drifter-like particles according to their temporal behavior.

The aim of this study was to validate the computational approach using existing documented data from the past search and rescue operation in the Mediterranean sea. In order to illustrate the application of the clustering algorithm, we used the Elba accident based on documented data from Italian Coast Guards. The Elba accident happened near to the Elba coast and in the Tyrrhenian Sea. During the accident, a person on an inflatable raft was lost at the coast of

the Elba Island at 42° 43.6′ N, 10° 9.5′ E on 21.06.2009 at 1:30 UTC and after 34 h, he was found alive in open sea southwards from the Pianosa Island at the position 42° 22.9′ N, 9° 53.3′ E, at the moment of rescue (22.06.2009 at 11:30 UTC), the boat was partially deflated. We used the modeling framework based on the explicit parameterization of an object drift by wind (Daniel et al. 2002; Hackett et al. 2006; Breivik and Allen 2008).

In the study, qualitative comparison between the behavior of reconstructed trajectories of sea objects and known information about the observed trajectory in the Elba accident was done using stochastic simulation of a large ensemble of identical drifter-like particles. In separate simulations, different categories of particles were tested to study the effect of wind on drifting direction and spatial distribution of probability densities. Application of the stochastic Leeway model (Breivik and Allen 2008) for tracking of small-size surface drifters was studied using geophysical forcing from the high-resolution Mediterranean Forecasting System (MFS) (Pinardi et al. 2003; Dobricic et al. 2004) and atmospheric wind from the European Centre for Medium-Range Weather Forecasts (ECMWF).

2 Model

The Leeway drift is defined as a drift of floating object with respect to ambient current under the influence of wind and waves (Chaplin 1960; Anderson et al. 1998; Breivik et al. 2012). According to the definition, the leeway velocity is a difference between the drift velocity of a sea object and Eulerian current velocity:

$$\mathbf{L} = \frac{d\mathbf{r}}{dt} - \mathbf{V}_E, \tag{1}$$

where $\mathbf{L}$ is Leeway velocity, $d\mathbf{r}/dt$ is the drift velocity, and $\mathbf{V}_E$ is the Eulerian current.

In the present implementation, we used the stochastic model based on the Eulerian leeway model (Breivik and

Table 1 Leeway coefficients for the categories: (1) life raft, shallow ballast (2) life raft, deep ballast, (3) surfboard with person, (4) sportsboat, (5) sport-fisher boat

Category	DWL			Right CWL			Left CWL		
	α_d	β_d,	σ_d	α_c	β_c,	σ_c	α_c	β_c	σ_c
1	2.68	0	12	1.1	0	9.4	−1.1	0	9.4
2	3.52	−2.5	6.1	0.62	−3	3.5	−0.45	−0.2	3.6
3	1.93	0	8.3	0.51	0	6.7	−0.51	0	6.7
4	6.54	0	3.0	2.19	0	2.8	−2.19	0	2.8
5	5.55	0	3.3	2.27	0	3	−2.27	0	3

The regression slope values $\alpha_{d,c}$ (%), the offset $\beta_{d,c}$ (cm/s), and the standard deviations $\sigma_{d,c}$ (cm/s) are shown for the DWL and the left/right CWL components. Values are provided from Allen and Plourde (1999)

Allen 2008; Röhrs et al. 2012). In particular, the equations of motion for a drifting object is derived from the force balance equation (Breivik and Allen 2008):

$$(m - m')\frac{d^2\mathbf{r}}{dt^2} = \mathbf{F}_{wave} + \mathbf{F}_{wind} + \mathbf{F}_{ocean}, \quad (2)$$

where m and m' are mass of object and an additive mass, $\mathbf{F}_{wind}$, $\mathbf{F}_{wave}$, and $\mathbf{F}_{ocean}$ are wind, wave, and water drags correspondingly. The expressions for wind and water drags of a small object are written as follows:

$$\mathbf{F}_{wind} = C_a \rho_a A_a \|\mathbf{W}_{10}\| \mathbf{W}_{10}, \quad (3)$$

$$\mathbf{F}_{ocean} = C_o \rho_o A_o \left| \mathbf{V}_L - \frac{d\mathbf{r}}{dt} \right| \left[\mathbf{V}_L - \frac{d\mathbf{r}}{dt} \right], \quad (4)$$

where $\mathbf{V}_L$ is the Lagrangian velocity of an object, $\mathbf{W}_{10}$ is 10 m atmospheric wind, $C_{a,o}$, $\rho_{a,o}$, and $A_{a,o}$ are drag coefficients, densities, and effective cross-sectional areas exposed to air and water correspondingly.

According to field observations, ships and small-size floaters reach terminal velocity rapidly (Sørgård and Vada 1998). Hence, an infinite acceleration and constant velocity at every time step can be assumed in Eq. 2 (Hodgins and Hodgins 1998). In the present modeling paradigm, a sea dominated by weak waves is considered. Also the damping and excitation by waves is neglected due to a small object size (Sørgård and Vada 1998; Breivik and Allen 2008). Based on these assumptions, Eq. 2 is simplified as follows (Anderson et al. 1998):

$$0 = \mathbf{F}_{wind} + \mathbf{F}_{ocean}, \quad (5)$$

Using the expressions for the wind and ocean forces from Eqs. 3–4, the equation of motion Eq. 2 can be written in the Eulerian leeway form (Breivik and Allen 2008):

$$d\mathbf{r} = (\mathbf{L} + \mathbf{V}_E)dt, \quad (6)$$

where $\mathbf{L} = \sqrt{C_a \rho_a A_a / C_o \rho_o A_o} \mathbf{W}_{10}$. Here, the relation $\mathbf{V}_L \approx \mathbf{V}_E$ (Röhrs et al. 2012) is used provided the wave effects could be neglected.

Since in our situation the drag coefficients were not known, the Leeway drift was parameterized using empirically derived relationship between the wind and Leeway velocity. First, the Leeway velocity was decomposed into downwind Leeway (DWL) L_d and crosswind Leeway (CWL) L_c projections: $\mathbf{L} = L_d \hat{w}_d + L_c \hat{w}_c$, where $\hat{w}_d$ and $\hat{w}_c$ are unit vectors parallel and perpendicular to wind direction correspondingly. Second, the following linear fit for the DWL and CWL derived from empirical relationship was used (Anderson et al. 1998; Allen and Plourde 1999; Breivik and Allen 2008):
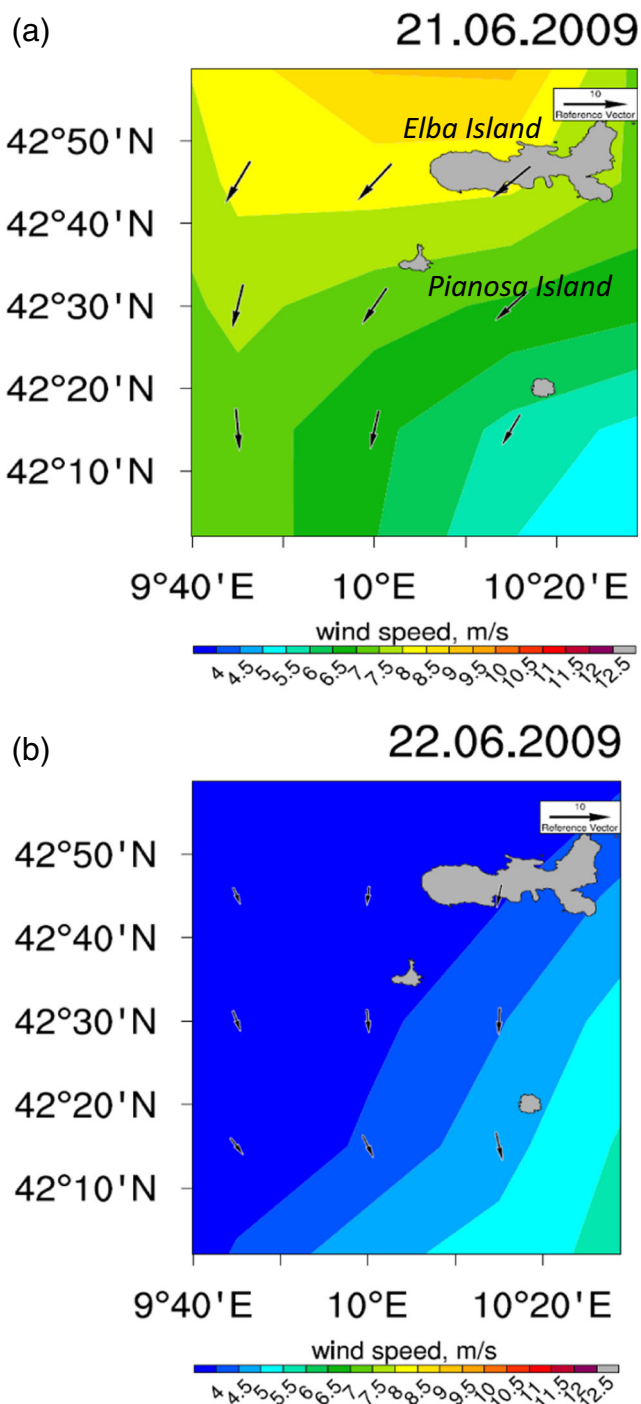
$$L_{d,c} = a_{d,c} W_{10} + b_{d,c}, \quad (7)$$

where a_d, b_d and a_c, b_c are the linear regression coefficients for L_d and L_c components, respectively, and $W_{10} = \sqrt{w_x^2 + w_y^2}$. The regression coefficients $a_{d,c}, b_{d,c}$ were

obtained by adding noise terms to linear regression coefficient from experimental observations (Allen and Plourde 1999):

$$a_{d,c} = \alpha_{d,c} + \zeta_{d,c}/20, \quad (8)$$

$$b_{d,c} = \beta_{d,c} + \zeta_{d,c}/2, \quad (9)$$

Fig. 2 Mean daily wind direction and magnitude from the ECMWF for days: **a** 21.06.2009 and **b** 22.06.2009. The wind data are from the ECMWF

where $\alpha_{d,c}$, $\beta_{d,c}$ are regression slope and offset terms obtained from empirical data (Allen and Plourde 1999), The noise terms $\zeta_{d,c}$ were derived from a normal distribution with the experimental value of variance $\sigma_{d,c}$ obtained from the field data (Allen and Plourde 1999). Finally, we calculated the Cartesian coordinates of **L** and substituted the values into Eq. 6.

To include the variabilities of the wind and Eulerian current velocities, the Gaussian perturbations were added at every integration step t_n and for the kth particle:
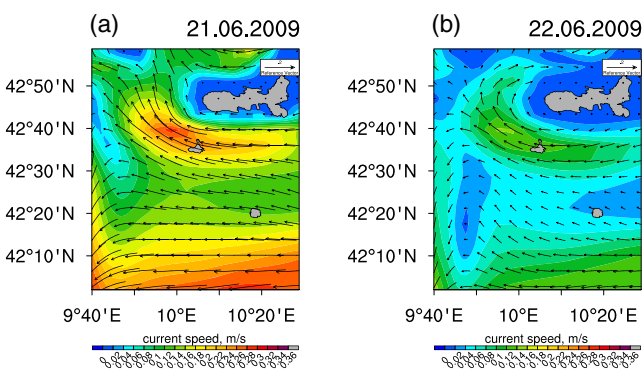
$$v_{x,y}(t_n, k) = v_{x,y}^{curr} + \xi_{x,y}^{curr}, \qquad (10)$$

$$w_{x,y}(t_n, k) = w_{x,y}^{wind} + \xi_{x,y}^{wind}, \qquad (11)$$

where $\xi_{x,y}^{curr}$ and $\xi_{x,y}^{wind}$ are the uncertainties derived from normal distributions $N(0, \sigma_{curr})$ and $N(0, \sigma_{wind})$ correspondingly.

Also, because of existing uncertainty of initial orientation of a sea object with respect to wind, an initial ensemble of particles was generated with random (left or right) initial orientation with respect to wind (Breivik and Allen 2008). The change of orientation was introduced via the alternation of sign of L_c with the probability 4 % per integration step (Allen 2005).

Due to a finite size of geographical domain, the particles could reach the boundary of the domain or approach coastal shoreline. In the former case, they were marked as off-grid and removed from further consideration. Stranded particles were identified according to a high-resolution coastline (Wessel and Smith 1996). In real situations, an uncertainty about the place and time of an accident might be present due to luck of information. To account for the uncertainties in the position of an accident, initial positions were assigned from a normal distribution centered around an expected location of an accident. Particularly, the particles were released continuously in a spatial area bounded by initial distance $r_0 = 0.5\sigma_r$ around the last known position (LKP), where σ_r is the variance of drifters initial positions.

The LKP refers to the possible location of an accident and is provided in terms of longitude and latitude for every particle.

We used the ECMWF fields with the horizontal and temporal resolutions of $0.25° \times 0.25°$ and 6 h, respectively. For the surface current, we used daily averages from the MFS model (horizontal resolution $0.0625° \times 0.0625°$) that is
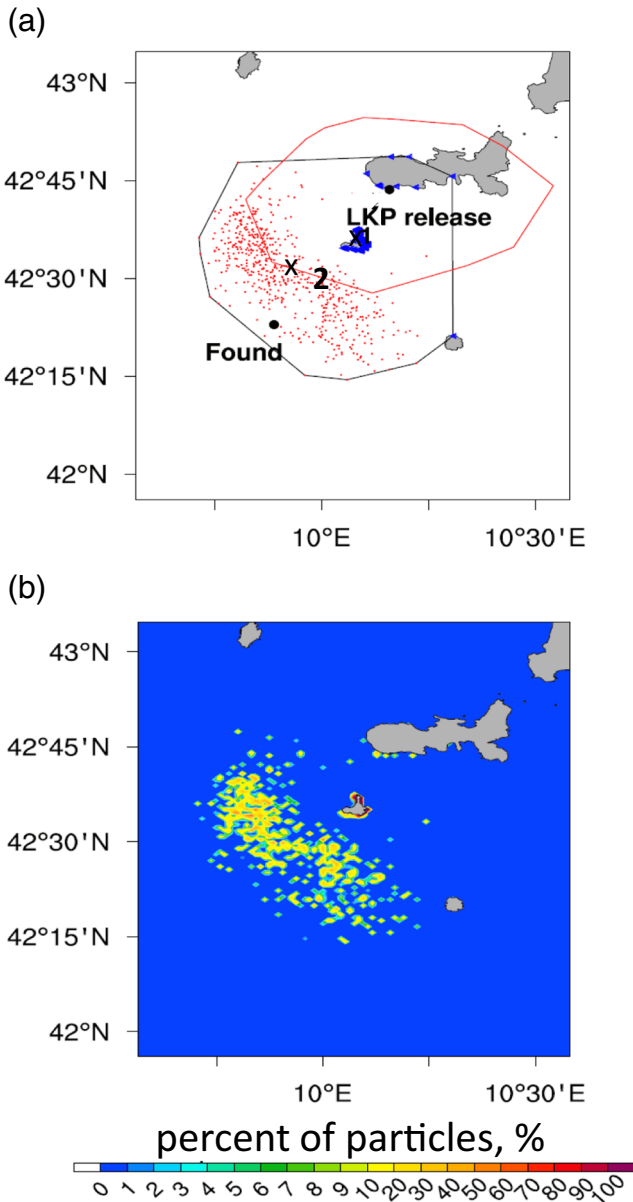
(a)

(b)

percent of particles, %
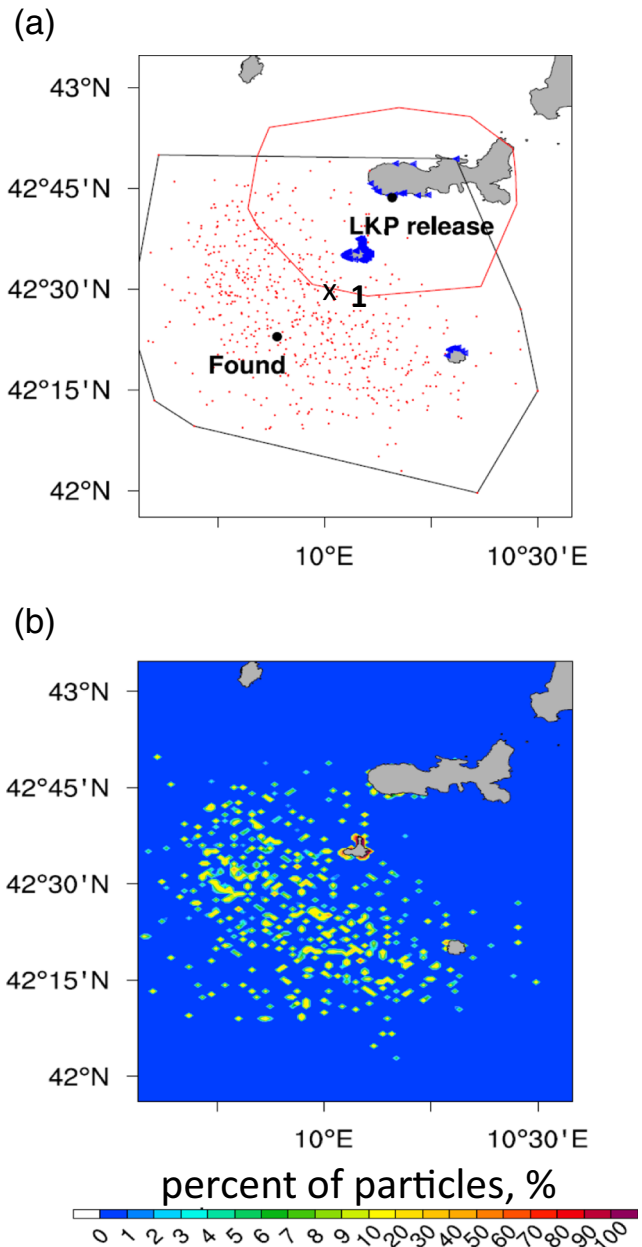
Fig. 4 Results of Leeway simulations for life raft with a shallow ballast: **a** final positions of particles, LKP (42° 43.6′ N, 10° 9.5′ E), rescue position (position where the person was found)(42° 22.9′ N, 9° 53.3′ E) (*black dots*), final positions (*red dots*) in open sea and (*blue triangles*) stranded on coast, initial area of release (*red convex polygon*), final area of search (*black convex polygon*), center of mass of cluster (*cross*); **b** spatial concentration (%) of particles. A single cluster **1** with all drifters included is distinguished

Fig. 3 Daily surface currents (direction and magnitude) for days: **a** 21.06.2009 and **b** 22.06.2009. The surface current is from the MFS

based on the ECMWF six-hourly fields and the data assimilation scheme (Pinardi et al. 2003; Dobricic et al. 2004; Dobricic and Pinardi 2008). Additionally, to provide a horizontal interpolation of the ocean currents and winds near to a shoreline, a sea-over-land interpolation procedure was implemented. The values for standard deviation (std) of wind $\sigma_{wind} = 2.8$ m s^{-1} and current $\sigma_{curr} = 0.1$ m s^{-1} in Eqs. 10–11 were estimated using averages over the corresponding geographical domain for the period of integration. The particle trajectories were obtained using Eq. 6 with the integration step d$t = 1.5$ min.

3 Methods

In the implementation of the clustering algorithm, the final positions of particle trajectories were used for evaluation of a spatial separation between them. The mean separation distance D_{mean} was evaluated across all pairs of ensemble members using formula:

$$D_{mean} = \frac{1}{N_{dr}} \sum_{\substack{i,j=1, \\ i \neq j}}^{N_{dr}} d_{ij}, \tag{12}$$

Fig. 5 Results of Leeway simulations for life raft with a deep ballast: **a** final positions of particles with initial release and final search areas, **b** spatial concentration (%) of particles. Two clusters are found: (*1*) stranded particles $\rho_{cl} = 7.62$ % and (*2*) open sea particles $\rho_{cl} = 92.1$ %
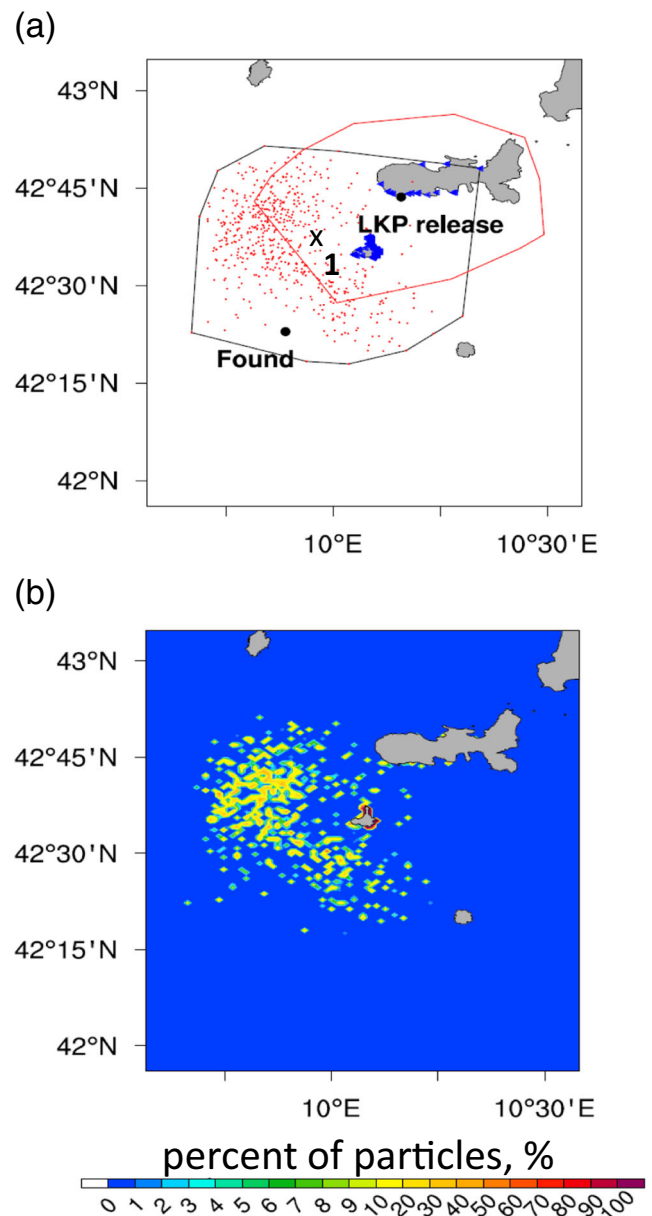
Fig. 6 Results of Leeway simulations for surfboard with person: **a** final positions of particles with initial release and final search areas, **b** spatial concentration (%) of particles. A single cluster is formed

and d_{ij} is an inter–particles distance evaluated from the Haversine formula:

$$d_{ij} = 2R_{\oplus} \arcsin \left[(f(\phi_1, \phi_2) + \cos\phi_i \cos\phi_j f(\lambda_i, \lambda_j))^{1/2} \right], \quad (13)$$

where $R_{\oplus}$ is the Earth radius, N_{dr} is ensemble size, and λ_i, ϕ_i are longitudes and latitudes of the ith particle and $f(x_1, x_2) = \sin^2 [(x_1 - x_2)/2]$. Also an upper bound D_{max} was assigned to exclude large mean separation distance that

exceeds the size of a given geographical domain. Indeed, in the case $D_{mean} > D_{max}$, no clusters were searched due to large inter-particle distance.

For the ith drifter, a new cluster was formed by the inclusion of the kth neighbor provided that the condition $d_{ik} < D_{mean}$ was satisfied. In addition, the minimal number of particles N_{min} forming one cluster was assigned that allowed exclusion of the search areas of lower density (in the simulations $N_{min} = 20$). The procedure was finalized after sorting all possible pairs of particles.
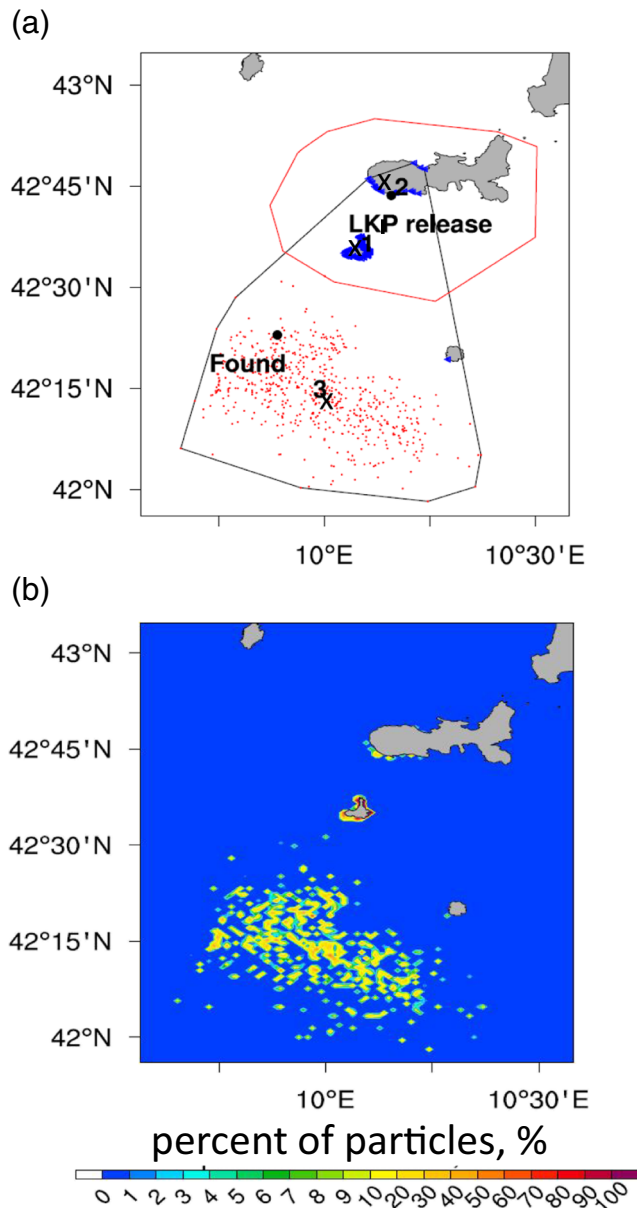
Fig. 7 Results of Leeway simulations for sport-fisher boat: **a** final positions of particles with initial release and final search areas, **b** spatial concentration (%) of particles. Three clusters are found: (*1*) stranded particles on the Pianosa coast $\rho_{cl} = 19.8$ %, (*2*) stranded particles near to the LKP $\rho_{cl} = 6.1$%, and (*3*) open sea particles $\rho_{cl} = 73.1$ %.
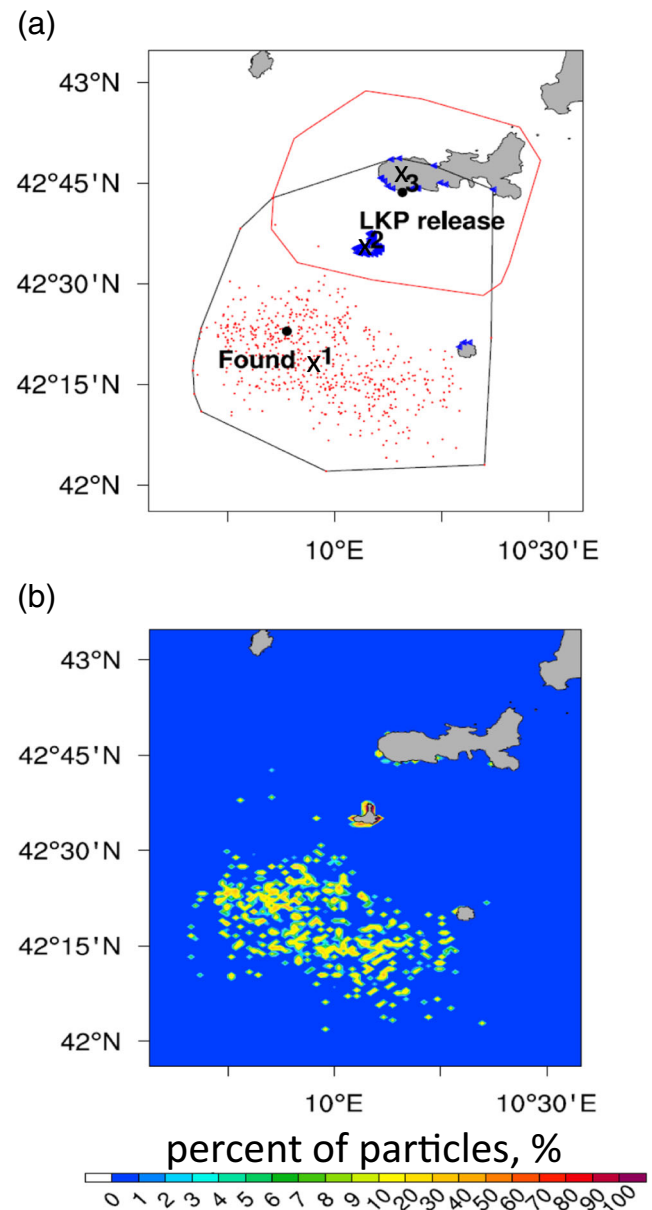
Fig. 8 Results of Leeway simulations for sports boat: **a** final positions of particles with initial release and final search areas, **b** spatial concentration (%) of particles. Three clusters are found: (1) open sea particles $\rho_{cl} = 72.8$ %, (2) stranded particles $\rho_{cl} = 19.6$ % and (3) stranded near to the LKP $\rho_{cl} = 7.2$ %

Table 2 Listed are the mean cluster position (latitude and longitude), number of clusters N_{cl} and probability of containment ρ_{cl} (%) for every cluster and experiment

Exp.	N_{cl}	Mean cluster position	ρ_{cl}, (%)
1	1	42°30′34″N 10°0′11″E	100
2	1	42°35′12″N 10°5′37″E	92.1
	2	42°28′43″N 9°55′24″E	7.62
3	1	42°35′45.4″N 9°56′53″E	100
4	1	42°34′53.7″N 10°4′58″E	19.8
	2	42°45′34″N 10°10′4″E	6.1
	3	42°13′7″N 10°0′11″E	73.1
5	1	42°16′18″N 9°56′14″E	72.8
	2	42°34′36″N 10°3′58″E	19.6
	3	42°45′48″N 10°10′20″E	7.2

The clustering algorithm is schematically illustrated in Fig. 1. Only the first group of particles is classified as one cluster. Although the second group includes two neighbors which are at the distance less than D_{mean} they do not form one cluster due to insufficient number of particles per cluster $N_k < 10$. The third group contains isolated particle that has no neighbors at a distance less than D_{mean} therefore it does not belong to any cluster.

In order to identify the search areas with higher density of particles, we classified a probability of containment ρ_{cl} [%] of particles per cluster: $\rho_{cl} = N_k/N_{dr} \times 100$ %, where N_k is a number of particles inside the kth cluster. The mean cluster geographical position (center of mass of the cluster) at every time step is defined from the mean latitude $\bar{\phi} = \sum_i \phi_i/N_{dr}$ and mean longitude $\bar{\lambda} = \sum_i \lambda_i/N_{dr}$ across all cluster members $i = 1, \ldots N_{dr}$.

Since the exact parameterization of the object was not known, the simulations of drifter-like particles were performed using the categories similar to a person on an inflatable boat (see Table 1). The ensemble of $N_{dr} = 3000$ particles was released in a circle with radius $r_0 = 15$ km around the LKP (42° 43.6′ N, 10° 9.5′ E). The time of the release of particles, radius r_0 and LKP were the same in all the experiments.

4 Results

The wind situation and mean surface current (Figs. 2 and 3) for 2 days of study period indicated an overall southwestern wind influence for the day 21.06.2009 (Fig. 2a) and the westward surface current contribution (Fig. 3a) to initial southwestern displacement of particles with respect to the release area (Figs. 4, 5, 6, 7, and 8). On the second day the decrease of mean surface current (Fig. 3b) and change of the wind direction (Fig. 2b) favored a slight shift of drift of trajectories to the southeast (Figs. 4, 5, 6, 7, and 8).

The results of cluster analysis show the release area of particles around the LKP, the search areas and final positions obtained from particle trajectories (Fig. 4a). Thus, the

final serach areas include the last time stamp from the particle trajectory for every particle. The initial area includes not only particles near to the LKP but also some coastal particles with zero initial velocities that remained beached or traveled short distances from the position of release. The spatial density map (Fig. 4b) indicates a higher percentage of particles near to the coastal area.

In the first experiment for the life raft with a shallow ballast (Fig. 4a), the search area included the found position, but the particles positions were distributed over a large area and, thus, their average density (Fig. 4b) around the found position was low. A significant percentage of particles was stranded on the Pianosa Island while the particles with low initial velocities were beached near to the LKP. In the next two experiments performed for two categories (i) raft with a deep ballast (Fig. 5) and (ii) person on a surfboat (Figs. 6), an overall southwestern drift from the LKP was observed. Two clusters were found for (i) with larger cluster formed by open sea particles ($\rho_{cl} = 92.1$ %) (see Table 2). In the last two experiments (Figs. 7 and 8) performed for draft-limited vessels (sport-fisher boat and sportsboat), the southwards direction of drift was more pronounced. The simulated trajectories more closely reproduced the target trajectory and found position than the trajectories in the previous experiments. Moreover, the search areas (Figs. 7 and 8) included the position of rescue with the largest clusters formed around it: for sportsboat cl. 1 with 72.8 % particles and for sport-fisher boat cl. 3 with 73.1 % particles (Table 2).

5 Discussion and conclusions

We observed high sensitivity of trajectories to the choice of wind category: the trajectories of particles with higher DWL and lower CWL more closely reproduced the target trajectory in terms of its drift direction. The draft-limited floaters with higher DWL were more influenced by the wind-induced forcing during test experiments. In contrast,

the particles modeling floaters with a deep draft were less affected by wind and drifted westwards from the Elba location. The clustering procedure helped identifying high density search areas that closely matched the final target position.

In the experiments, all particles were released simultaneously. Generally, uncertainty in time also could be included (Breivik and Allen 2008). According to numerical procedure, the final search area depends on the initialization area of the particles: higher r_0 LKP leads to increased variability in the trajectories of drift and, therefore, to the larger search area. In our experiments, sufficiently large radius around LKP ($r_0 = 15$ km) was used to detect all possible directions of drift as well as existing clusters.

In contrast to previous numerical procedures (Breivik and Allen 2008), the approach developed here enabled determination of spatially isolated search areas and classification of the particles according to distinct trajectory behavior. The sorting of trajectories is especially important for the geophysical flows with inherent hyperbolic points that are strain dominated. In particular, the Lagrangian particles released in the closed vicinity of the hyperbolic point would diverge rapidly. Thus, the probability of a successful search could be substantially reduced due to large search areas. However, this limitation could be successfully avoided by application of clustering method that reduces the final search domains and classifies distinct directions of drift.

Our modeling paradigm could be used for the development of reliable computer-assisted approach for the search and rescue operational systems. Our approach was used to assist recent sea emergencies: (i) the accident near the Lampedusa Island (3.10.2013–8.10.2013), and (ii) the sea operations on the elevation of the Costa Concordia cruise ship (16.09.2013–19.09.2013) at the east of Giglio Island, the Tyrrhenian Sea. In the former case, we helped to reconstruct the accident and to identify possible locations of lost people during the emergency response by the Italian Coast Guards. In the latter case, the method provided the forecast of drift as well as potential positions of ship wreckage pieces.

At present, the method described here is used in the first prototype of the search and rescue operational system in the Mediterranean region http://www.ocean-sar.com/en/discover-sar.

Appendix

The Leeway coefficients for the categories used in the experiments are provided here. The slope, offset, and std for the CWL, DWL are given in Table 1.

References

Allen AA (2005) Leeway divergence, USCG *R*&; D Center technical report CG-D-05-05. Available through http://www.nts.gov

Allen AA, Plourde JV (1999) Review of leeway: Field experiments and implementation. Technical report CG-D-08-99, US Coast Guard Research and Development Center. Groton, CT, USA

Allen A, Roth JC, Maisondieu C, Breivik Ø, Forest B (2010) Field determination of the Leeway of Drifting Objects. Technical Report 17/2010, Norwegian Meteorological Institute

Anderson E, Odulo A, Spaulding M (1998) Modeling of Leeway drift. U. S. Coast Guard Research and Development Center. Report No. CG-D-06-99

Breivik Ø, Allen AA (2008) An operational search and rescue model for the Norwegian Sea and the North Sea. J Mar Syst 69(1–2):99–113. doi:10.1016/j.jmarsys.2007.02.010

Breivik Ø, Allen AA, Maisondieu C, Roth J-C, Forest B (2012) The leeway of shipping containers at different immersion levels. Ocean Dyn 62:741–752. doi:10.1007/s10236-012-0522-z

Chaplin WE (1960) Estimating the drift of distressed small craft. Coast Guard Alumni Association Bulletin, U.S. Coast Guard Academy. New London, CT 22(2):39–42

Daniel P, Jan G, Cabioch F, Landau Y, Loiseau E (2002) Drift modeling of cargo containers. Spill Sci Technol B 7(5–6):279–288. doi:10.1016/S1353-2561(02)00075-0

Davidson FJM, Allen A, Brassington GB, Breivik Ø, Daniel P, Kamachi M, Sato S, King B, Lefevre F, Sutton M, Kaneko H (2009) Application of GODAE ocean current forecasts to search and rescue and ship routing. Oceanography 22(3):176–181. doi:10.5670/oceanog.2009.76

Dobricic S, Pinardi N, Adani M, Bonazzi A, Fratianni C, Tonani M (2004) Mediterranean Forecasting System: a new assimilation scheme for sea level anomaly and its validation. Q J R Meteorol Soc 128:1–12

Dobricic S, Pinardi N (2008) An oceanographic three-dimensional variational data assimilation scheme. Ocean Model 22:89–105. doi:10.1016/j.ocemod.2008.01.004

Ester M, Kriegel H-P, Sander J, Xu X (1996) A density–based algorithm for discovering clusters in large spatial databases with noise. In: Simoudis E, Han J, Fayyad UM (eds) Proceedings of the Second International Conference on Knowledge Discovery and Data Mining (KDD-96). AAAI Press, pp 226–231

Hackett B, Breivik Ø, Wettre C (2006). In: Chassignet EP, Verron J (eds) Forecasting the drift of objects and substances in the oceans, pp 507–524

Hodgins DO, Hodgins LM (1998) Phase II Leeway Dynamics Program: Development and Verification of a Mathematical drift model for liferafts and small boats. Report, Canadian Coast Guard, Nova Scotia, Canada

Kirwan AD, McNally G, Chang M-S, Molinari R (1975) The effects of winds and surface currents on drifters. J Phys Oceanogr 5:361–368

Oddo P, Pinardi N, Zavatarelli M, Coluccelli A (2006) The Adriatic Basin Forecasting System. Acta Adriat 47(Suppl):169–184

OD́onnell L, Ullman D, Spaulding M, Howeless T, Fake P, Hall P et al (2005) Integration of coastal ocean Short-Term Predictive System (STPS) Surface Current estimates into the search and rescue optimal planning system., http://www.rdc.uscg.gov

Pinardi N, Allen I, Demirov E, De Mey P, Korres G, Lascaratos A, Le Traon P-Y, Maillard CG, Manzella G, Tziavos C (2003) The Mediterranean ocean forecasting system: first phase of implementation (1998-2001). Ann Geophys 21:3–20. doi:10.5194/angeo-21-3-2003

Röhrs J, Christensen KH, Hole LR, Broström G, Drivdal M, Sundby S (2012) Observation-based evaluation of surface wave effects on currents and trajectory forecasts. Ocean Dynam 62:1519–1533. doi:10.1007/s10236-012-0576-y

Sørgård E, Vada T (1998) Observations and modelling of drifting ships. DNV Technical Report 96–2011, Det norske Veritas, Hovik, Norway

Tonani M, Pinardi N, Dobricic S, Pujol I, Fratianni C (2008) A high resolution free surface model on the Mediterranean sea. Ocean Sci 4:1–14. doi:10.5194/os-4-1-2008

Wessel P, Smith WHF (1996) A global, selfconsistent, hierarchical, high-resolution shoreline database. J Geophys Res 101(B4):8741–8743